# Critical current of a quasi-one-dimensional superconducting wire

Li-Fu Chang, Santanu Chaudhuri, and Philip F. Bagwell
*School of Electrical and Computer Engineering, Purdue University, West Lafayette, Indiana 47907*
(Received 29 November 1995)

We solve the Bogoliubov–de Gennes equations self-consistently to obtain the critical current $I_c$ versus Fermi energy $\mu$ for a ballistic quasi-one-dimensional superconducting wire. Instead of the ''discretized'' critical current $I_c(\mu)=Ne\Delta_{\rm bulk}/\hbar$ predicted for a superconducting point contact, we find $I_c(\mu)=[4e\Delta_{\rm wire}(\mu)/h][n(\mu)/n_1(\mu)]$ for the superconducting wire. The normalized electron density $n(\mu)/n_1(\mu)=\Sigma_{i=1}^{N}(k_{Fi}/k_{F1})\leqslant N$ is a slowly increasing function of $\mu$. The superconducting order parameter $\Delta_{\rm wire}(\mu)$ must be obtained self-consistently for each value of the Fermi energy. We find $\Delta_{\rm wire}(\mu)$ follows the normal-metal quasi-one-dimensional density of states $N(\mu)$ of the wire, as does the critical current $I_c(\mu)$ .

## I. INTRODUCTION

Recently Beenakker and van Houten[1] have predicted the ''discretization'' of the critical current in a superconducting point contact in units of $e\Delta_{\rm bulk}/\hbar$, where $2\Delta_{\rm bulk}$ is the energy gap of the bulk superconductors. Reference 1 has stimulated much additional work on the electrical characteristics of superconducting weak links.[2–20] Several of these recent works[14–20] have also emphasized the importance of satisfying the self-consistency requirement for the order parameter $\Delta(r,\mu)$ in superconductors subject either to a current flow or spatial variations in geometry. Satisfying the self-consistency condition for $\Delta(r,\mu)$ is necessary both to predict the critical current in any geometry and to ensure electrical current conservation.[15–18] The multimoded superconducting wire we consider in this paper illustrates several effects the self-consistency condition for $\Delta(r,\mu)$ has on electronic transport in restricted geometries.

We compare the superconducting point contact and superconducting wire geometries in Fig. 1. Reference 1 argues that, because the electrical current density is geometrically diluted in a point contact, the order parameter for the bulk superconductor $\Delta_{\rm bulk}$ cannot greatly change when connected to another bulk superconductor through a point contact. For the point contact, the self-consistency requirement then has minimal effect on the critical current, as numerically confirmed in Ref. 14. We therefore choose to study a superconducting wire geometry, where several coherence lengths $\xi_0$ separate the bulk superconducting reservoirs terminating the wire. The electrical current density is uniform along the length of the wire, and is not geometrically diluted until reaching the distant superconducting reservoirs. The superconducting order parameter $\Delta_{\rm wire}$ in the wire can then differ greatly from the bulk order parameter $\Delta_{\rm bulk}$, as determined from the self-consistency condition. Determining the order parameter $\Delta_{\rm wire}$ requires solving a multiple mode Bogoliubov–de Gennes (BdG) equation described in Sec. II.

The resulting critical current $I_c(\mu)$ of the superconducting point contact and superconducting wire are shown schematically in Fig. 1. The critical current of the point contact increases in ''discretized'' increments whenever the Fermi energy crosses a confinment subband energy $E_1,E_2,E_3,\ldots$ . In contrast, we find in Sec. III that the dependence of critical current on Fermi energy $\mu$ in the superconducting wire resembles the electronic density of states of the normal-metal wire $N(\mu)$. That the superconducting order parameter follows the density of states is well known from the superconductivity of uniform thin films,[21] small metallic islands, and fullerines.[22] The critical current of the quasi-one-dimensional (Q1D) wire is proportional to the energy gap $\Delta_1$ of the lowest subband, i.e., $\Delta_{\rm wire}\equiv\Delta_1$, as described in Sec. IV.

Although one cannot directly vary the Fermi energy $\mu$ in a metallic superconducting wire to observe $I_c(\mu)$, the same qualitative variation of $I_c(B)$ could be observed by depopulating the subbands with an applied magnetic field $B$. The resulting $I_c(B)$ will be an interplay of the Pauli depairing, orbital depairing, and depopulating of the confinement subbands. The variation of order parameter and critical current can also be observed by varying the wire width as suggested in Ref. 21. In clean, type-I superconducting wire, which is wide enough such that phase slippage does not limit the critical current, it should be possible to observe quantum con-

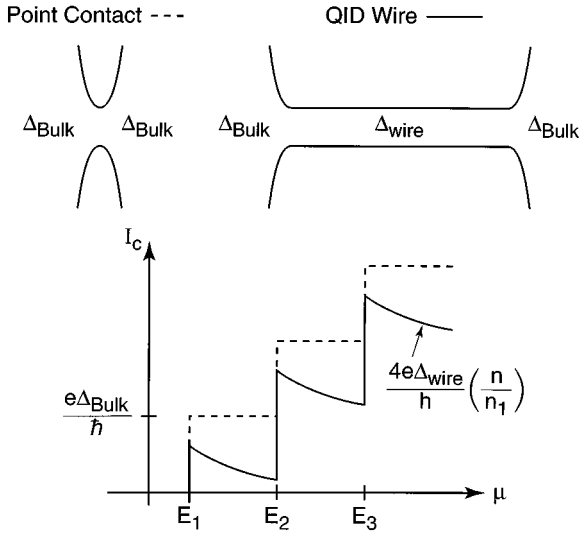


FIG. 1. Model geometry of a superconducting point and a superconducting quasi-one-dimensional wire. The $I_c$ versus $\mu$ relation of the point contact (dashed) increases in steps whenever $\mu$ exceeds a confinement subband minima $E_1$, $E_2$, $E_3$, etc. $I_c(\mu)$ for the superconducting wire (solid) follows the density of modes $N(\mu)$ of the wire in its normal state.

 © 1996 The American Physical Society

finement effects on the critical current and superconducting density of states.

## II. MULTIPLE MODE BdG EQUATION

The BdG equations[23,24] describe the electron motion in a superconducting structure according to

$$\begin{pmatrix} H(x,y)-\mu & \Delta(x,y) \\ \Delta^*(x,y) & -[H^*(x,y)-\mu] \end{pmatrix} \begin{pmatrix} u_p(x,y) \\ v_p(x,y) \end{pmatrix} = E_p \begin{pmatrix} u_p(x,y) \\ v_p(x,y) \end{pmatrix}. \tag{1}$$

We take the coordinate $x$ to vary along the length of the wire, and $y$ to describe spatial variation along the wire width. The one-electron Hamiltonian function $H(x,y)$ in Eq. (1)

$$H(x,y)=H_0(x,y)+V_c(y), \tag{2}$$

describes free electron motion with $H_0(x,y)$ and the lateral confinement potential with $V_c(y)$. Here $H_0(x,y)$ is

$$H_0(x,y)=\frac{1}{2m}\left(-i\hbar\frac{d}{dx}-eA_x\right)^2+\frac{1}{2m}\left(-i\hbar\frac{d}{dy}-eA_y\right)^2. \tag{3}$$

For a uniform superconducting wire, the ordering parameter $\Delta(x,y)$ will have the form

$$\Delta(x,y)=\Delta(y)e^{2iqx}. \tag{4}$$

The magnitude $\Delta(y)$ of the ordering parameter varies only along $y$ because the wire is uniform in the $x$ direction. We can further take $\Delta(y)$ to be a real number, since no supercurrent will flow along $y$. The phase gradient of the ordering parameter $2q$ determines the superfluid flow velocity $v_s=\hbar q/m$,[15] allowing the wire to carry a supercurrent along the $x$ direction. The order parameter $\Delta(x,y)$ in Eq. (1) must be calculated self-consistently from[23]

$$\Delta(y)e^{2iqx}=-g(x,y)\sum_p v_p^*(x,y)u_p(x,y)f(E_p) \times\theta(\hbar\omega_D-|E_p|). \tag{5}$$

Here $f(E_p)=1/[1+\exp(E_p/k_BT)]$ is the Fermi occupation factor. Any coupling constant $g(x,y)=g(y)>0$ favors superconductivity. We cut off the summations in Eq. (5) for $|E_p|>\hbar\omega_D$, where $\omega_D$ is the Debye frequency.

The electrical current $I_Q$ we find by first evaluating the electrical current density operator[15]

$$J_Q(y)=\sum_p [J_{u_p}+J_{v_p}]f(E_p)-\sum_p J_{v_p}. \tag{6}$$

The $J_u$ and $J_v$ are the Schrödinger currents associated with the waves $u_p$ and $v_p$, namely $J_{u_p}=e(\hbar/m)\mathrm{Im}[u_p^*(x,y)\nabla_x u_p(x,y)]$ and $J_{v_p}=e(\hbar/m)\mathrm{Im}[v_p^*(x,y)\nabla_x v_p(x,y)]$. The total current $I_Q$ flowing in the $x$ direction is obtained by summing $J_Q(y)$ along the width of the wire

$$I_Q=\int J_Q(y)dy. \tag{7}$$

Note that the summations in Eq. (5) and Eq. (6) are carried out over all $E_p$, including $E_p<0$.

We choose a harmonic oscillator confinement potential

$$V_c(x)=\frac{1}{2}m\omega_0^2y^2 \tag{8}$$

to represent the quasi-one-dimensional wire. If the wire width is much smaller than the London penetration depth, so that an applied magnetic field penetrates the wire uniformly, we can also adopt a vector potential $A_x=-By$ and $A_y=0$. The magnetic field is perpendicular to the wire as $\vec{B}=B\hat{z}$. The confining potential $V_c(x)$ and the vector potential $\vec{A}$ restrict the electrons to propagate via magnetoelectric subbands.[25] In the normal state the subband energies are $E_n=\hbar\omega(n-\frac{1}{2})$, where $\omega^2=\omega_0^2+\omega_c^2$ and $\omega_c=eB/m$ is the cyclotron frequency. Here $n=1,2,3,\ldots,$ denote the first, second, etc., subbands.

Assuming the wire is uniform along the $x$ direction, the eigenstate in Eq. (1) has the solution form

$$\begin{pmatrix} u_p(x,y) \\ v_p(x,y) \end{pmatrix}=\begin{pmatrix} C_p(y)e^{iqx} \\ D_p(y)e^{-iqx} \end{pmatrix}e^{ikx}. \tag{9}$$

In this problem we can take the quantum number $p=(k,\beta)$, where $k$ is the wave number and $\beta$ the band index. Inserting Eq. (9) into Eq. (1) yields

$$\begin{pmatrix} H_+(y) & \Delta(y) \\ \Delta^*(y) & -H_-(y) \end{pmatrix}\begin{pmatrix} C_p(y) \\ D_p(y) \end{pmatrix}=E_p\begin{pmatrix} C_p(y) \\ D_p(y) \end{pmatrix}, \tag{10}$$

where

$$H_+(y)=-\frac{\hbar^2}{2m}\frac{d^2}{dy^2}+\frac{m}{2}\omega^2(y-y_+)^2+\alpha_+, \tag{11}$$

$$H_-(y)=-\frac{\hbar^2}{2m}\frac{d^2}{dy^2}+\frac{m}{2}\omega^2(y+y_-)^2+\alpha_-, \tag{12}$$

$$y_\pm=-\frac{\hbar\omega_c(k\pm q)}{m\omega^2}, \tag{13}$$

and

$$\alpha_\pm=\frac{\hbar^2}{2m}(k\pm q)^2\frac{\omega_0^2}{\omega^2}-\mu. \tag{14}$$

We expand the wave functions $C_p(y)$ and $D_p(y)$ of the superconducting wire in Eq. (10) as a linear combination of harmonic oscillator basis states $\Psi_n(y)$ of the normal wire as

$$\begin{pmatrix} C_p(y) \\ D_p(y) \end{pmatrix}=\sum_n \begin{pmatrix} u_{pn}\Psi_n(y-y_+) \\ v_{pn}\Psi_n(y+y_-) \end{pmatrix}. \tag{15}$$

The $\Psi_n(y)$'s diagonalize the harmonic confinement potential as[26]

$$\left[-\frac{\hbar^2}{2m}\frac{d^2}{dy^2}+\frac{m}{2}\omega^2y^2\right]\Psi_n(y)=E_n\Psi_n(y), \tag{16}$$

with $\Psi_n(y)$ the standard Hermite-Gaussian wave functions. Inserting Eq. (15) into Eq. (10), and using the orthonormality of the $\Psi_n(y)$'s, yeilds a Hermitian matrix equation for the eigenenergies $E_p$ and expansion coefficients $(u_{pn},v_{pn})$

$$(E_m+\alpha_+)u_{pm}+\sum_n \Delta_{mn}v_{pn}=E_p u_{pm}$$

$$\sum_n \Delta^*_{nm}u_{pn}-(E_m+\alpha_-)v_{pm}=E_p v_{pm}, \tag{17}$$

derived in Appendix A. Equations similar to Eq. (17) have been used to describe the layered high-$T_c$ compounds.[27] Writing Eq. (17) explicitly for a quasi-one-dimensional wire with only two subbands gives

$$\begin{pmatrix} E_1+\alpha_+ & \Delta_{11} & 0 & \Delta_{12} \\ \Delta^*_{11} & -(E_1+\alpha_-) & \Delta^*_{21} & 0 \\ 0 & \Delta_{21} & E_2+\alpha_+ & \Delta_{22} \\ \Delta^*_{12} & 0 & \Delta^*_{22} & -(E_2+\alpha_-) \end{pmatrix} \times \begin{pmatrix} u_{p1} \\ v_{p1} \\ u_{p2} \\ v_{p2} \end{pmatrix} = E_p \begin{pmatrix} u_{p1} \\ v_{p1} \\ u_{p2} \\ v_{p2} \end{pmatrix}. \tag{18}$$

Here $\Delta_{mn}$ is a matrix element of the ordering parameter $\Delta(y)$ with the harmonic oscillator basis states as

$$\Delta_{mn}=\int_{-\infty}^{\infty}\Psi^*_m(y-y_+)\Delta(y)\Psi_n(y+y_-)dy. \tag{19}$$

The off-diagonal matrix elements $\Delta_{mn}$ in Eqs. (19) couple the electron in subband $m$ and the time-reversed electron mode $n$, an ''intersubband Andreev reflection'' due to spatial variation in the order parameter $\Delta(y)$. The particle density normalization condition requires

$$\int_{-\infty}^{\infty}\int_{-\infty}^{\infty}dxdy[|u_p(x,y)|^2+|v_p(x,y)|^2]$$

$$=1=\sum_n [|u_{pn}|^2+|v_{pn}|^2]. \tag{20}$$

We can express the ordering parameter $\Delta(y)$ from Eq. (5) in terms of the expansion coefficients in Eq. (17) as

$$\Delta(y)=-g(y)\sum_p \sum_{mn} u_{pm}v^*_{pn}\Psi_m(y-y_+) \times\Psi^*_n(y+y_-)f(E_p)\theta(\hbar\omega_D-|E_p|). \tag{21}$$

Similarly, the electrical current densities $J_u(y)$ and $J_v(y)$ expressed in terms of the expansion coefficients in Eq. (17) are

$$J_{u_p}(y)=e\frac{\hbar(k+q)}{m}\left|\sum_n u_{pn}\Psi_n(y-y_+)\right|^2 \tag{22}$$

and

$$J_{v_p}(y)=e\frac{\hbar(k-q)}{m}\left|\sum_n v_{pn}\Psi_n(y+y_-)\right|^2. \tag{23}$$

The electrical current is then obtained from Eq. (6) by integrating Eqs. (22) and (23) over the cross section as

$$I_Q(y)=\sum_p [I_{u_p}+I_{v_p}]f(E_p)-\sum_p I_{v_p}. \tag{24}$$

For $B=0$, the case we consider in this paper,[28] the currents $I_{u_p}$ and $I_{v_p}$ have the simple form

$$I_{u_p}=e\frac{\hbar(k+q)}{m}\sum_n |u_{pn}|^2 \tag{25}$$

and

$$I_{v_p}=e\frac{\hbar(k-q)}{m}\sum_n |v_{pn}|^2. \tag{26}$$

Starting from an initial guess for the ordering parameter $\Delta(y)$, and for a given value of the superfluid velocity $v_s$, we compute the eigenvalues and eigen vectors of Eq. (17). The solution of Eq. (17) generates a new pairing potential $\Delta(y)$ according to Eq. (21), etc. We iterate this process until $\Delta(y)$ from Eq. (21) converges to self-consistency with Eq. (17). We then calculate the electrical current $I_Q$ for this given value of the superfluid velocity $v_s$ from Eqs. (24)–(26). The critical current is found from by varying the superfluid velocity $v_s$ until the maximum $I_Q$ is reached at each Fermi level $\mu$, namely

$$I_c(\mu)=\max I_Q(v_s,\mu). \tag{27}$$

## III. ENERGY GAPS AND CRITICAL TEMPERATURE

In this section we calculate the pairing potential $\Delta(y)$, the dispersion relation $E_\beta(k)$, the superconducting energy gap $\Delta_1(\mu)$ for the first subband, and the corresponding critical temperature $T_c(\mu)$. The coupling constant is taken to be $g(y)=g_{2D}=$constant.[29] We have assumed a Q1D wire having three normal modes. As long as we limit the Fermi energy to $\mu<E_4$, increasing the number of modes will not qualitatively affect the result of the calculations.

The self-consistency condition for the superconducting pairing potential $\Delta(y)$, Eq. (21), forces it to vary along the width of the wire. The self-consistent $\Delta(y)$ at zero temperature and zero supercurrent flow $(q=0)$ is shown in Fig. 2 for (a) one and (b) two occupied subbands. In Fig. 2(a) the Fermi energy is halfway between the first and second subbands, $\mu_1=(E_1+E_2)/2$. Similarly, the Fermi energy is $\mu_2=(E_2+E_3)/2$ in Fig. 2(b). The spatial variation of $\Delta(y)$ in Fig. 2 follows the spatial variation of the electron density $|\Psi_n(y)|^2$ in each lateral mode. For two occupied subbands in Fig. 2(b), $\Delta(y)$ is wider and more spatially uniform than for one occupied subband in Fig. 2(a). When many subbands are occupied, so that $\mu$ is large, $\Delta(y)$ will be approximately constant and the subbands will almost completely decouple.

The dispersion diagram for two occupied subbands in a superconducting wire subject to a superfluid flow is shown in Fig. 3. The first subband $(\beta=\pm1)$ is shown as a solid line in Fig. 3, while the second subband $(\beta=\pm2)$ is the dotted line.

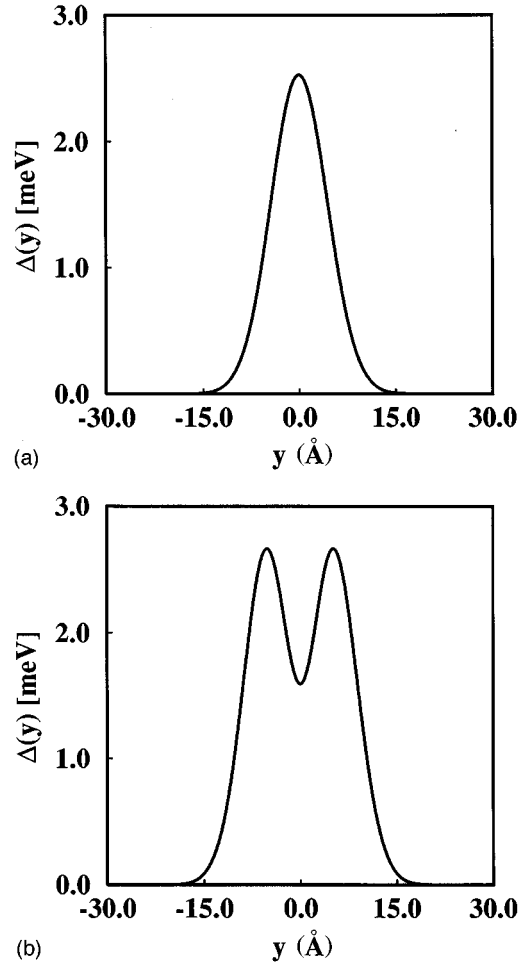


FIG. 2. Self-consistent order parameter $\Delta(y)$ when (a) one or (b) two subbands are occupied. $\Delta(y)$ follows the electron density $n(y)$ of each populated confinement subband.

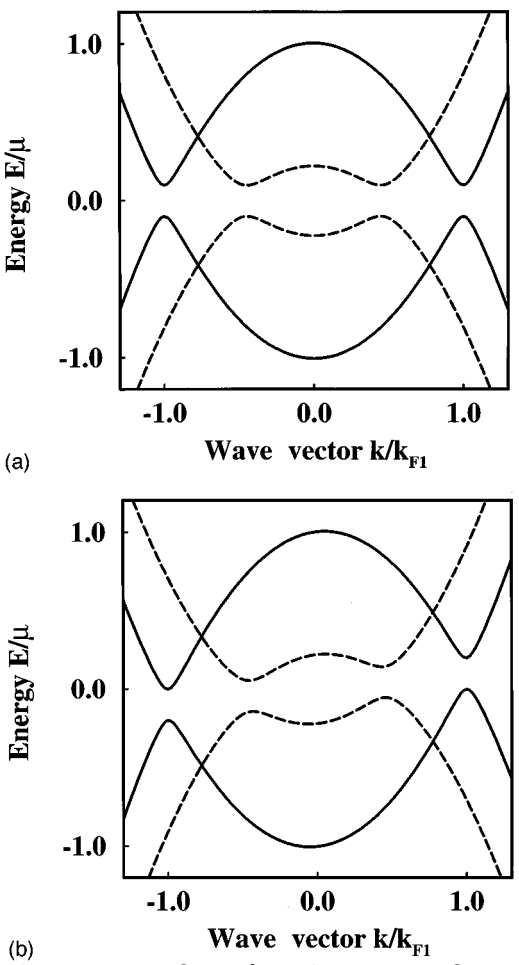


FIG. 3. Dispersion relation for a Q1D superconductor having two occupied subbands. An energy gap for the first (solid) and second (dashed) electronic subbands opens when each subband crosses the Fermi level. The superfluid velocity is zero in (a), i.e., $q=0$. The presence of a superfluid flow ''tilts'' the energy bands in (b).

Energy gaps are opened in Fig. 3 where each subband crosses the Fermi level. The energy gap near $E=0$ and wave vector $k_{F1}$ we define as $\Delta_1$, the energy gap for the first subband. Here the Fermi wave vector is

$$p_{Fm}=\hbar k_{Fm}=\sqrt{2m(\mu-E_m)}. \tag{28}$$

Similarly, $\Delta_2$ is the energy gap of the second subband, which opens near $E=0$ and wavevector $k_{F2}$. We choose a large $\Delta_1/\mu$ ratio in Fig. 3 so the energy gaps are visible.[30]

There are small ''intersubband'' energy gaps away from the Fermi level in Fig. 3, where the energy bands cross each other, not visible in the figure. Again due to the slow spatial variation of $\Delta(y)$, the intersubband matrix elements $\Delta_{mn}$ for $m\neq n$ are small. If $\Delta(y)$ were actually constant across the wire, we would then have $\Delta_{mn}=0$ for $m\neq n$, and the modes would completely decouple. Because the mode coupling is small, and hence $\Delta_{12}\simeq 0$, $\Delta_{21}\simeq 0$, etc., we have from Eq. (18) that $\Delta_1(\mu)\simeq\Delta_{11}$, $\Delta_2(\mu)\simeq\Delta_{22}$, etc. References 1–20 either explicitly restrict the electron transport to be one dimensional, or assume the electronic subbands decouple in the narrowest portion of the wire or weak link, so that electrons in the different electronic confinement subbands superconduct independently. For the *s*-wave superconducting wire we consider in this paper, we find this mode coupling is not significant, so that the subbands do in fact superconduct essentially independently. If a magnetic field is applied, or the narrow superconductor has a *d*-wave or other unconventional order parameter, the mode coupling can become significant.

We also find generally that the energy gaps of each subband at the Fermi level are approximately the same, namely $\Delta_1(\mu)\simeq\Delta_2(\mu)=\cdots$. The spatial variations in $\Delta(y)$, generated from Eq. (21), turn out again not to be rapid enough to make the energy gaps very different. Reference 21 reaches the same conclusion for a thin *s*-wave superconducting film. For the current carrying superconductor in Fig. 3(b), the energy gaps opening at each subband for a fixed $k$ remain approximately constant. However, the band structure in Fig. 3(b) is now ''tilted'' due to the superfluid flow.[15] This ''tilting'' corresponds to a shift of the Fermi surface by an amount $q$ in $k$ space (momentum space).

Figure 4 shows the self-consistent $\Delta_1(\mu)$ when the superfluid velocity is zero ($q=0$). $\Delta_1(\mu)$ in Fig. 4 follows the quasiparticle density of states $N(\mu)$ of a normal-metal Q1D wire, incrasing sharply just above each subband minima at $\mu=E_n$ and decaying as $\mu$ approaches the next subband minima. We can understand this result from the self-consistency condition for the ordering parameter $\Delta(y)$ in Eq.

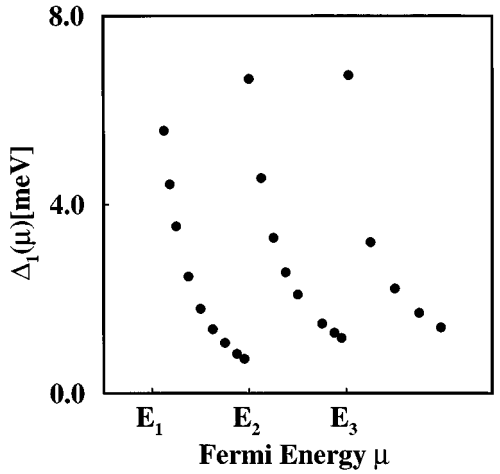


FIG. 4. Energy gap $\Delta_1(\mu)$ of the lowest confinement subband. $\Delta_1(\mu)$ follows the normal-metal density of states $N(\mu)$ of the wire.

(21). Because we take the Debye energy range in Eq. (21) to be narrow compared to the subband spacing ($\hbar\omega_D \ll \hbar\omega_0$), Eq. (21) simply counts the number of states in the energy range $\hbar\omega_D$ near $\mu$ with a weighting factor $u_{pm}v_{pn}^*\Psi_m(y-y_+)\Psi_n^*(y+y_-)$. Although this weighting factor will vary somewhat with Fermi energy, $\Delta(y,\mu)$ basically follows the normal-metal density of states $N(\mu)$ of the narrow wire. $\Delta_1(\mu)$ then also follows the density of states $N(\mu)$, since $\Delta_1$ averages $\Delta(y)$ along the width of the wire. Although the normal-metal density of states has a singularity at each subband opening, $\Delta_1(\mu)$ does not become infinite near a subband minima. We give a more quantitative analysis for $\Delta_1(\mu)$ when only a single subband is occupied in Appendix B.

That the energy gap $\Delta_1(\mu)$ follows the normal-metal density of states $N(\mu)$ can be also reasoned from the BCS theory.[31] The BCS result for the energy gap of a one-dimensional superconductor is

$$\Delta_1(\mu) = \frac{\hbar\omega_D}{\sinh[1/gN(\mu)]}. \tag{29}$$

In the strong coupling limit $gN(\mu) \gg 1$, Eq. (29) becomes

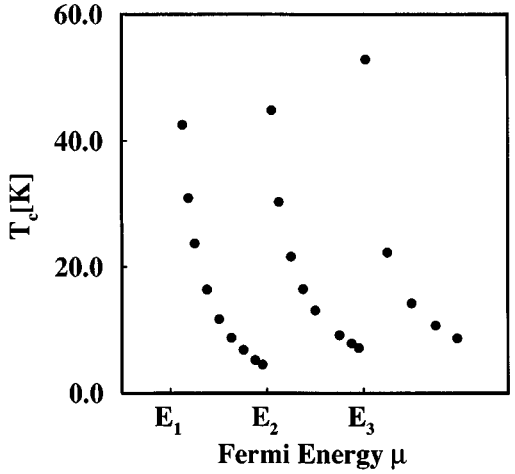


FIG. 5. Critical temperature $T_c(\mu)$. $T_c(\mu)$ also follows the normal-metal density of states $N(\mu)$ of the wire.

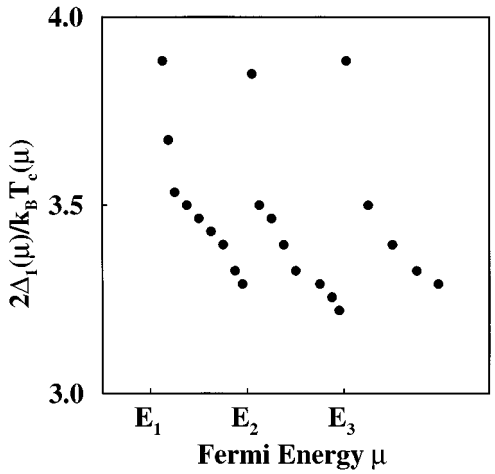


FIG. 6. Ratio $R = 2\Delta_1(\mu)/k_BT_c(\mu)$ versus $\mu$ from Fig. 3 and 4. $R$ remains close to the BCS value of $R \simeq 3.5$, having a maximum value slightly less than four above each subband opening.

$$\Delta_1(\mu) \simeq \hbar\omega_D gN(\mu), \tag{30}$$

which is directly proportional to the density of states. Of course, even in the weak-coupling limit $gN(\mu) \ll 1$, where

$$\Delta_1(\mu) \simeq 2\hbar\omega_D/\exp[1/gN(\mu)], \tag{31}$$

the energy gap still increases if the density of states increases.

The critical temperature $T_c$ for the Q1D wire is obtained when the temperature $T \geqslant T_c$ forces the ordering parameter $\Delta(y)$ to be zero, depairing the wire. We plot the numerical result for $T_c$ as a function of Fermi energy $\mu$ at zero superfluid flow ($q=0$) in Fig. 5. The dependence of $T_c(\mu)$ in Fig. 5 is similar to $\Delta_1(\mu)$ from Fig. 4. Both $T_c(\mu)$ and $\Delta_1(\mu)$ follow the density of states $N(\mu)$. We can compare $T_c(\mu)$ and $\Delta_1(\mu)$ by forming the ratio $R = 2\Delta_1(\mu)/k_BT_c$, shown in Fig. 6. For a weak-coupling BCS superconductor $R \simeq 3.5$. However, we see from Fig. 6 that $R$ remains near 3.5, even when $\mu$ is near the singular density of states at each subband opening. Reference 32 introduces a singular density of states in the BCS theory, finding $R \leqslant 4$. We find $R$ has a maximum value slightly less than 4 at each subband opening, so that Fig. 6 agrees with Ref. 32.

## IV. CRITICAL CURRENT

We show the electrical current $I_Q$ versus superfluid velocity $v_s = \hbar q/m$ in Fig. 7. As in the one-dimensional case,[15] the electrical current increases linearly with $v_s$. Because all subbands are essentially independent current carrying channels driven by the same pairing potential $\Delta(x,y)$, we can write

$$I_Q \simeq ev_s n = ev_s \sum_{i=1}^{N} n_i, \tag{32}$$

where $n_i$ is the electron density in subband $i$. Again, as for the one-dimensional case,[15] the order parameter $\Delta_1(\mu,q) \simeq \Delta_1(\mu,q=0)\,\theta(q_c - |q|)$ remains approximately constant with $q$ until the critical velocity $q_c$.

Figure 7 also shows that the critical superfluid velocity $v_{c1}$ for $\mu_1 = (E_1+E_2)/2$ (one occupied subband) and $v_{c2}$ for

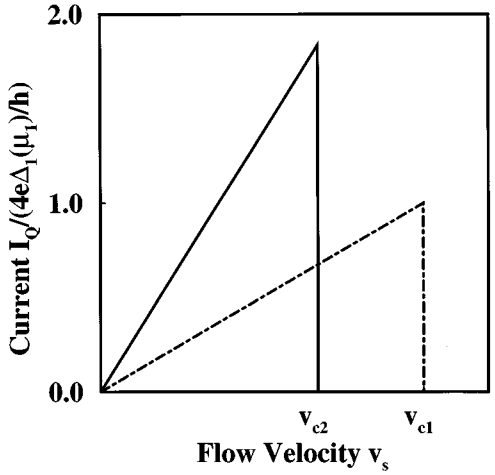


FIG. 7. Electrical current $I_Q$ versus superfluid flow velocity $v_s$ for one (dashed) and two (solid) occupied subbands. The critical superfluid velocity $v_c$ is smaller when two subbands are occupied, $v_{c2}<v_{c1}$. This is because $v_c$ is limited by the energy gap and Fermi momentum of the lowest subband as $v_c=\Delta_1(\mu)/p_{F1}(\mu)$.

$\mu_2=(E_2+E_3)/2$ (two occupied subbands). That the critical superfluid velocity $v_c$ is smaller when the Fermi energy is in the second subband, $v_{c2}<v_{c1}$, can be understood qualitatively from Fig. 3(b). When only one subband is occupied, we have the Landau depairing velocity (Ref. 33) $v_c=\Delta_1/p_{F1}$ as in Ref. 15. For several occupied subbands, the energy gap $(\Delta E)_i$ of each subband will close as

$$(\Delta E)_i=\Delta_i(q=0)-v_s p_{Fi}. \tag{33}$$

Since the energy gaps $\Delta_i(q=0)$ for all the subbands are approximately the same, and since $p_{F1}$ is the largest Fermi momentum, the energy gap of the first subband will close for the smallest value of $q$.

When the energy gap of the first subband closes, superconductivity in the wire is completely destroyed. This depairing condition $(\Delta E)_1=0$ occurs at a superfluid velocity

$$v_c=\frac{\Delta_1(\mu)}{p_{F1}(\mu)} \tag{34}$$

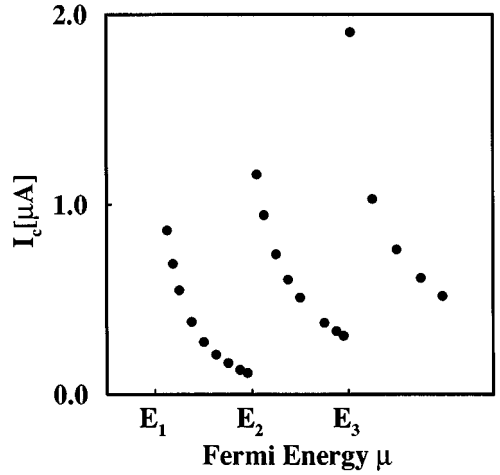


FIG. 8. Critical current $I_c(\mu)$ versus Fermi energy $\mu$ relation. The data points obtained from Eq. (22) match the analytical results of Eq. (33). $I_c(\mu)$ also follows the normal-metal density of states $N(\mu)$ of the wire.

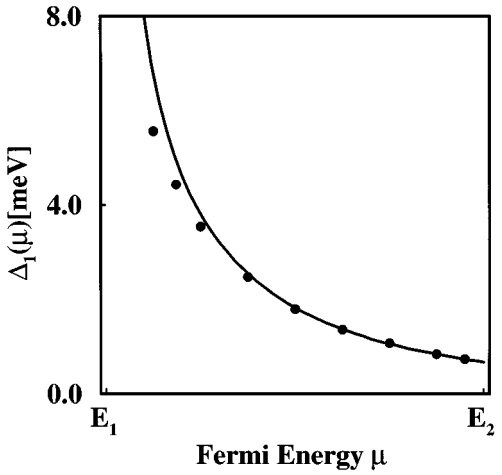


FIG. 9. Energy gap $\Delta_1(\mu)$ for a single occupied subband computed from the approximate Eq. (B10) (solid) and from Fig. 4. The small difference arises from the different method of imposing the Debye energy cutoff in Eq. (B10).

for all values of the Fermi energy $\mu$. The depairing condition is shown graphically in Fig. 3(b), where the band edge of the first subband touches the Fermi level when $v_s=v_c$. The energy gap for the lowest subband $(\Delta E)_1=0$ has closed in Fig. 3(b), while the energy gap of the second subband remains open $(\Delta E)_2>0$. Using Eq. (34), the larger Fermi momentum when two subbands are occupied, $p_{F1}(\mu_2)>p_{F1}(\mu_1)$, explains why $v_{c2}=[\Delta_1(\mu_2)/p_{F1}(\mu_2)]<v_{c1}=[\Delta_1(\mu_1)/p_{F1}(\mu_1)]$ in Fig. 7. Further, since the $\Delta_1(\mu)$ is the relevant energy gap which determines the critical current in Eq. (34), we can define $\Delta_{\rm wire}(\mu)=\Delta_1(\mu)$. [For a nonequilibrium superconductor[18,19] the depairing condition might not be given by Eq. (34), though we know of no specific example where this is the case.]

The critical current $I_c$ for $N$ propagating modes can now be written as

$$I_c=ev_c\sum_{i=1}^{N} n_i=ev_c n_1\sum_{i=1}^{N}(n_i/n_1)=\left(\frac{4e\Delta_1(\mu)}{h}\right)\left(\sum_{i=1}^{N}\frac{k_{Fi}}{k_{F1}}\right). \tag{35}$$

Here $n_i=2k_{Fi}/\pi$ is the quasiparticle density for the $i$th mode. Since the summation $\Sigma_{i=1}^{N}(n_i/n_1)\leqslant N$ is a slowly increasing function of $\mu$, we conclude that the more rapid variation of the self-consistent energy gap $\Delta_1(\mu)$ in Fig. 4 controls the dependence of the critical current $I_c(\mu)$ in Eq. (35). Therefore, $I_c(\mu)$ should also follow the one-dimensional normal-metal density of states $N(\mu)$. We plot the self-consistent $I_c(\mu)$ from Eq. (7) in Fig. 8. The data in Fig. 8 agree with in Eq. (35), using the self-consistent energy gap $\Delta_1(\mu)$ from Fig. 4 to evaluate Eq. (35).

## V. CONCLUSIONS

By solving the BdG equations, we have shown that the dependence of the energy gap $\Delta_1(\mu)=\Delta_{\rm wire}(\mu)$, the critical temperature $T_c(\mu)$, and the critical current $I_c(\mu)$ on the

Fermi energy $\mu$ in a Q1D superconducting wire follow the variation of the normal-metal density of states $N(\mu)$ with Fermi level. For example, the critical current $I_c(\mu)$ increases sharply just after the Fermi level crosses a Q1D subband energy at $\mu=E_n$. $I_c(\mu)$ then decreases with Fermi energy until crossing the next subband Q1D subband energy at $\mu=E_{n+1}$. This behavior of $I_c(\mu)$, $\Delta_1(\mu)$, and $T_c(\mu)$ is consistent with the BCS theory for the superconducting energy gap $\Delta_1(\mu)$ of a narrow superconductor. All physical quantities like $\Delta_1(\mu)$, $T_c(\mu)$, $I_c(\mu)$, should follow the normal-metal density of states $N(\mu)$ in a Q1D superconducting wire.

Analogous to the well-known result of Beenakker and van Houten[1] for the critical current of a superconducting point contact, $I_c(\mu)=Ne\Delta_{\rm bulk}/\hbar$, we have found for the Q1D superconducting wire that $I_c(\mu)=[4e\Delta_{\rm wire}(\mu)/h][n(\mu)/n_1(\mu)]$. Our result is different from Ref. 1 due to the different model geometries, a point contact in Ref. 1 versus a superconducting wire in this paper. The discretized $I_c(\mu)$ for a superconducting point contact should evolve into the $I_c(\mu)$ predicted in this paper for a Q1D superconducting wire as the length of the point contact increases. Even though the normal-state conductance $G(\mu)$ of the superconducting point contact and superconducting wire are identical, their critical currents $I_c(\mu)$ are quite different.

Differences in the two critical current formulas can be understood from the difference in point contact versus wire geometries. For the point contact, the order parameter of the bulk electrodes $\Delta_{\rm bulk}$ is essentially fixed as a function of Fermi energy. For the superconducting wire the bulk electrodes are far removed from the main body of the wire, so that $\Delta_{\rm wire}(\mu)$ must be calculated self-consistently for each Fermi energy $\mu$. Furthermore, due to the nonzero superfluid momentum in the wire, the effective channel number is reduced from $N$ for the point contact to the density ratio $n(\mu)/n_1(\mu)\leqslant N$ in the Q1D wire. This is because the Landau depairing velocity of the first subband, $v_c=\Delta_1(\mu)/p_{F1}(\mu)$, limits the critical current of the wire. Even though all subbands conduct essentially independently, higher Q1D subbands will carry less supercurrent than lower ones due to their smaller electron density, reducing the effective channel number.


## ACKNOWLEDGMENTS

We thank Supriyo Datta, Al Overhauser, and Richard Riedel for useful discussions. We acknowledge the supercomputing support from the National Center for Supercomputing Applications at University of Illinois at Urbana-Champagn, Illinois. We gratefully acknowledge financial support from the David and Lucile Packard Foundation.


## APPENDIX A: MULTIMODE BdG EQUATION

In this appendix we obtain the multimode BdG equation, Eq. (17). Substituting Eq. (15) into Eq. (10), we obtain

$$\begin{aligned}\int_{-\infty}^{\infty}dy\sum_n&\begin{pmatrix}\Psi_m^*(y-y_+)&0\\0&\Psi_m^*(y+y_-)\end{pmatrix}\\&\times\begin{pmatrix}H_+(y)&\Delta(y)\\\Delta^*(y)&-H_-(y)\end{pmatrix}\begin{pmatrix}u_{pn}\Psi_n(y-y_+)\\v_{pn}\Psi_n(y+y_-)\end{pmatrix}\\&=\int_{-\infty}^{\infty}dyE_p\sum_n\begin{pmatrix}\Psi_m^*(y-y_+)&0\\0&\Psi_m^*(y+y_-)\end{pmatrix}\\&\times\begin{pmatrix}u_{pn}\Psi_n(y-y_+)\\v_{pn}\Psi_n(y+y_-)\end{pmatrix}.\end{aligned}\tag{A1}$$

Using the eigenvalue equations

$$\begin{aligned}H_+(y)\Psi_n(y-y_+)&=(E_n+\alpha_+)\Psi_n(y-y_+),\\H_-(y)\Psi_n(y+y_-)&=(E_n+\alpha_-)\Psi_n(y+y_-),\end{aligned}\tag{A2}$$

and the orthonormality of the $\Psi_n$'s

$$\int_{-\infty}^{\infty}dy\Psi_m(y)\Psi_n(y)=\delta_{mn},\tag{A3}$$

we obtain from Eq. (A1)

$$\begin{aligned}(E_m+\alpha_+)u_{pm}+\sum_n\Delta_{mn}v_{pn}&=E_pu_{pm},\\\sum_n\tilde{\Delta}_{mn}^*u_{pn}-(E_m+\alpha_-)v_{pm}&=E_pv_{pm}.\end{aligned}\tag{A4}$$

In Eq. (A4) the $\Delta_{mn}$ and $\tilde{\Delta}_{mn}^*$ are

$$\begin{aligned}\Delta_{mn}&=\langle\Psi_m(y-y_+)|\Delta(y)|\Psi_n(y+y_-)\rangle\\\tilde{\Delta}_{mn}^*&=\langle\Psi_m(y+y_-)|\Delta^*(y)|\Psi_n(y-y_+)\rangle.\end{aligned}\tag{A5}$$

Taking the complex conjugate of $\Delta_{mn}$ in Eq. (40), we see that

$$(\Delta_{mn})^*=\tilde{\Delta}_{nm}^*.\tag{A6}$$

Substituting Eq. (A6) into Eq. (A4) yields Eq. (17) of Sec. II.

## APPENDIX B: $\Delta(y)$ FOR A SINGLE MODE

In this appendix we obtain a simplified self-consistent equation for $\Delta_1(\mu)$ when only one subband is occupied. When $E_1<\mu<E_2$ the wave function for the lowest subband $\Psi_1(y)$ is the dominant term in Eq. (9), so that

$$\begin{pmatrix}u_p(x,y)\\v_p(x,y)\end{pmatrix}\simeq\begin{pmatrix}u_{p1}\Psi_1(y)\\v_{p1}\Psi_1(y)\end{pmatrix}e^{ikx},\tag{B1}$$

where we have assumed $q=0$ and $B=0$. The dispersion law for the superconductor is then $E_p=\beta E_k$, with

$$E_k=\sqrt{E'^2+\Delta_1^2(\mu)},\tag{B2}$$

and the quantum number $\beta=\pm1$. The normal-state energy is $E'+\mu=\hbar^2k^2/2m$. The factors $u_1$ and $v_1$ in Eq. (B1) are the BCS coherence factors for a one-dimensional

superconductor[15] having the self-consistent energy gap $\Delta_1(\mu)$. Analysis of the wave functions themselves gives

$$u_{p1}v_{p1}=\frac{\Delta_1(\mu)}{2E_p}=\beta\frac{\Delta_1(\mu)}{2E_k}. \tag{B3}$$

Inserting Eqs. (B1)–(B3) into Eq. (21) gives

$$\Delta(y)=-g_{2D}\Psi_1^2(y)\sum_{k,\beta}\beta\frac{\Delta_1(\mu)}{2E_k}f(\beta E_k)\theta(\hbar\omega_D-E_k). \tag{B4}$$

Using

$$\Delta_1(\mu)\simeq\int_{-\infty}^{\infty}\Delta(y)\Psi_1^2(y)dy, \tag{B5}$$

we obtain the self-consistency condition

$$1=-g_{1D}\sum_{\beta=\pm1}\sum_{k}\beta\frac{1}{2E_k}f(\beta E_k)\theta(\hbar\omega_D-E_k), \tag{B6}$$

where the effective one-dimensional BCS coupling constant $g_{1D}$ is

$$g_{1D}=g_{2D}\int_{-\infty}^{\infty}\Psi_1^4(y)dy. \tag{B7}$$

Eq. (B7) is approximately $g_{1D}\simeq g_{2D}/W$ where $W$ is the wire width. Evaluating the $\Sigma_\beta$ with

$$f(E_k)-f(-E_k)=-\tanh\left(\frac{E_k}{2k_BT}\right) \tag{B8}$$

leaves

$$1=g_{1D}\sum_{k}\tanh\left(\frac{E_k}{2k_BT}\right)\frac{1}{2E_k}\theta(\hbar\omega_D-E_k). \tag{B9}$$

The normal-metal density of states $N(E')$ is defined by

$$\sum_{k}\rightarrow L_x\int_{-\infty}^{\infty}\frac{dk}{2\pi}\rightarrow\int_{-\infty}^{\infty}N(E')dE'. \tag{B10}$$

modifying Eq. (B9) to

$$1=g_{1D}\int_{-\infty}^{\infty}N(E')dE'\tanh\left(\frac{E_k}{2k_BT}\right)\frac{1}{2E_k}\theta(\hbar\omega_D-E_k). \tag{B11}$$

Provided $\hbar\omega_D\gg\Delta_1(\mu)$, we can place the energy cutoff on $E'$ directly to obtain

$$1=\frac{g_{1D}}{2}\int_{-\hbar\omega_D}^{\hbar\omega_D}N(E')dE'\tanh\left(\frac{\sqrt{E'^2+\Delta_1^2(\mu)}}{2k_BT}\right)\times\frac{1}{\sqrt{E'^2+\Delta_1^2(\mu)}}. \tag{B12}$$

We plot the solution $\Delta_1(\mu)$ of Eq. (B12) as the solid line in Fig. 9. In Fig. 9 the $\Delta_1(\mu)$ values from solving Eq. (B12) agree well with the exact $\Delta_1(\mu)$ from Eq. (21). The small difference arises from how one applies the energy cutoff $\hbar\omega_D$. Eq. (B12) uses $|E'|\leqslant\hbar\omega_D$, while the numerical simulation in Fig. 9 uses $|E_p|\leqslant\hbar\omega_D$. If we had instead used the energy cutoff $|E'|\leqslant\sqrt{(\hbar\omega_D)^2-\Delta_1^2}$ in Eq. (B12), we would obtain much better agreement with the numerical simulation.


[1] C.W.J. Beenakker and H. van Houten, Phys. Rev. Lett. **66**, 3056 (1991).

[2] B.J. van Wees, K.M.H. Lenssen, and C.J.P.M. Harmans, Phys. Rev. B **44**, 470 (1991).

[3] C.W.J. Beenakker, Phys. Rev. Lett. **67**, 3836 (1991).

[4] C.W.J. Beenakker, in *Proceedings of the 14th Taniguchi International Symposium on ''Physics of Mesoscopic Systems''*, edited by H. Fukuyama and T. Ando (Springer, Berlin, 1992).

[5] A. Furusaki, H. Takayanagi, and M. Tsukada, Phys. Rev. Lett. **67**, 132 (1991); A. Furusaki, H. Takayanagi, and M. Tsukada, Phys. Rev. B **45**, 10 563 (1992).

[6] P.F. Bagwell, Phys. Rev. B **46**, 12 573 (1992).

[7] G.E. Rittenhouse and J.M. Graybeal, Phys. Rev. B **49**, 1182 (1994).

[8] M. Hurd and G. Wendin, Phys. Rev. B **49**, 15 258 (1994).

[9] L. Chang and P.F. Bagwell, Phys. Rev. B **49**, 15 853 (1994).

[10] See the collection of articles in *Proceedings of the NATO Advanced Research Workshop on Mesoscopic Superconductivity*, edited by F.W.J Hekking, G. Schon, and D.V. Averin [Physica B **203**, 201 (1994)].

[11] U. Gunsenheimer and A.D. Zaikin, Phys. Rev. B **50**, 6317 (1994).

[12] D. Averin and A. Bardas, Phys. Rev. Lett. **75**, 1831 (1995).

[13] M. Hurd, S. Datta, and P.F. Bagwell, Phys. Rev. B **54**, 6557 (1996).

[14] A. Martin-Rodero, F.J. Garcia-Vidal, and A. Levy Yeyati, Phys. Rev. Lett. **72**, 554 (1994); A. Levy Yeyati, A. Martin-Rodero, and F.J. Garcia-Vidal, Phys. Rev. B **51**, 3743 (1995).

[15] P.F. Bagwell, Phys. Rev. B **49**, 6841 (1994).

[16] R. A. Riedel, L. Chang, and P. F. Bagwell, Phys. Rev. B (to be published).

[17] A. Furusaki and M. Tsukada, Solid State Commun. **78**, 299 (1991).

[18] F. Sols and J. Ferrer, Phys. Rev. B **49**, 15 913 (1994).

[19] A. Martin and C.J. Lambert, Phys. Rev. B **51**, 17 999 (1995).

[20] J. Sánchez Cañizares and F. Sols, J. Phys. Condens. Matter **7**, L317 (1995).

[21] J.M. Blatt and C.J. Thompson, Phys. Rev. Lett. **10**, 332 (1963).

[22] J. Friedel, J. Phys. (France) II **2**, 959 (1992).

[23] P.G. deGennes, *Superconductivity of Metals and Alloys* (Addison-Wesley, New York, 1989).

[24] S. Datta, P.F. Bagwell, and M.P. Anantram, Phys. Low Dimensional Struct. **3**, 1 (1996).

[25] S. Datta, *Electronic Transport in Mesoscopic Systems* (Cambridge University Press, Cambridge, 1995).

[26] L.I. Schiff, *Quantum Mechanics* (McGraw-Hill, New York, 1971), Chap. 4.

[27] W.A. Atkinson and J.P. Carbotte, Phys. Rev. B **52**, 6894 (1995).

[28] N. Dupuis and G. Montambaux, Phys. Rev. B **49**, 8993 (1994).

[29] As our initial guess for the ordering parameter we take $\Delta(y)=\Delta_0=$const. = 1 meV. The confining potential strength is $\hbar\omega_0$ = 200 meV, making the effective width $W$ of the wire no larger than 30 Å. The mass $m$ is the free electron mass, yielding $E_1=100$ meV, $E_2=300$ meV, and $E_3=500$ meV. We use $g_{2D}=2.0\times10^{-38}$ J−m$^2$ and $\hbar\omega_D=10$ meV. In Fig. 2 and Fig. 7, the Fermi level is (a) $\mu=200$ meV and (b) $\mu=400$ meV.

[30] We choose a set of parameters in Fig. 3 that are different from the other figures, so one can clearly see the detail of the energy gaps and dispersion law.

[31] J. Bardeen, L.N. Cooper, and J.R. Schrieffer, Phys. Rev. **104**, 1189 (1957).

[32] D.C. Mattis and M. Molina, Phys. Rev. B **44**, 12 565 (1991); S. Takács, Phys. Rev. B **46**, 3145 (1992).

[33] L. Landau, J. of Phys. (USSR) **5**, 71 (1941), Sec. 4.